First Joint Congress on Fuzzy and Intelligent Systems
Ferdowsi University of Mashhad, Iran
29-31 Aug 2007

Semi-active Control of Structures Using Neuro-Inverse Model of MR Dampers

A. Khajekaramodin
Dept. of Civil Eng.
Ferdowsi University
a -karam@gmail.com

H. Haji-kazemi
Dept. of Civil Eng.
Ferdowsi University
hkazemi@ferdowsi.um.ac.ir

A. Rowhanimanesh
Dept. of Electrical Eng
Ferdowsi University
rowhanimanesh@gmail.com

M-R. Akbarzadeh
Dept. of Electrical Eng
Ferdowsi University
akbarzadeh@ieee.org

Abstract: A semi-active controller-based neural network for nonlinear benchmark structure equipped with a magnetorheological (MR) damper is presented and evaluated. An inverse neural network model (NIMR) is constructed to replicate the inverse dynamics of the MR damper. Linear quadratic Gaussian (LQG) controller is also designed to produce the optimal control force. The LQG controller and the NIMR models are linked to control the structure. The effectiveness of the NIMR is illustrated and verified using simulated response of a full-scale, nonlinear, seismically excited, 3-story benchmark building excited by several historical earthquake records. The semi-active system using the NIMR model is compared to the performance of an active and a clipped optimal control (COC) system, which are based on the same nominal controller as is used in the NIMR damper control algorithm. The results demonstrate that by using the NIMR model, the MR damper force can be commanded to follow closely the desirable optimal control force. The results also show that the control system is effective, and achieves better performance than active and COC system.

Keywords: Structural Control, Semi-active, Neural Network, Nonlinear, MR Damper

1 Introduction

The magnetorheological (MR) damper is generating a great interest among researchers in semi-active control of civil structures [1-6]. The MR damper is smart semi-active control device that generates force to a given velocity and applied voltage. The MR damper filled with a special fluid that includes very small polarizable particles that can change its viscosity rapidly from liquid to semi-solid and vice versa by adjusting the magnitude of the magnetic field produced by a coil wrapped around the piston head of the damper. The magnetic field can be tuned by varying the electrical current sent into the coil. When no current is supplied, the MR damper behaves similar to ordinary viscous damper, whereas its fluid starts to change to semi-solid as the current is gradually sent through the coil. Consequently, semi-active control using MR dampers are powerful devices that enjoy the advantages of passive devices with the benefits of active control. Additionally, they are inherently stable, reliable, and relatively cost-effective; they require small activation power.

One challenge in the use of semi-active technology is in developing nonlinear control algorithms that are appropriate for implementation in full-scale structures. Numerous control algorithms have been adopted for semi-active systems. These algorithms are either conventional methods based on mathematical formulation [1-6] or intelligent methods based on neural networks or fuzzy logic [7–12].

Interest in a new class of computational intelligence systems known as artificial neural networks (ANNs) has grown in the last few several years. This type of network has been found to be a powerful computational tool for organizing and correlating information in ways that have been proven to be useful for solving certain types of problems that are complex and poorly understood. The applications of ANNs to the area of structural control have grown rapidly through system identification, system inverse identification or controller replication [7-9].

In addition to using linear quadratic regulator (LQR) method, Chang and Zhou [13] manipulated recurrent neural networks to emulate the inverse dynamics of the MR damper to predict the required voltage for full-state feedback closed-loop system. This model used to control a three-storey building subjected to El Centro earthquake record. Similarly, Bani-Hani and Mashal [8] proposed neural network to simulate the inverse model of an MR damper in a 6-story base-isolated building subjected to earthquake forces.

In this paper, a NN model is used to emulate the inverse dynamics of the MR damper. This NN model is trained based on the input–output data generated using the phenomenological model proposed by Dyke et al. [14]. The model calculates a voltage signal based on a few previous time steps of velocity, damper force, and the desirable control force. This NN model is used to calculate voltage signals to be input to the MR damper so that it can produce desirable optimal control forces that is estimated by LQG control algorithm. In principle, these control forces can come from any control algorithm that requires an explicit use of control forces to mitigate response.

2 Three-Story Benchmark Building

The benchmark buildings of 3-story used for this study were designed for the Los Angeles region as defined by Ohtori et al. [15], in the problem definition paper. The building is 36.58 by 54.87 m in width, and 11.89 m in height. Two far-field and two near-field historical ground motion records are selected for study: El Centro 1940, Hachinohe 1968, Northridge 1994, and Kobe 1995 earthquakes. Control actuators are located on each floor of the structure to provide forces to adjacent floors. Because the actuator capacity is limited to a maximum force of 1,000 kN, three actuators are employed at the first floor and two actuators at both the second and the third floors to provide the required larger forces. Three sensors for acceleration measurements are used for feedback in the control system on the first, second, and third floors.

3 Control Strategy

Figure 1 illustrates the proposed control strategy. There is basically no restriction on the type of control algorithm that should be used as long as it calculates a desirable control force f_d based on response and/or excitation. The desirable control force and the response of the building are passed in to the inverse NN model. This NN model emulates inverse dynamics of the MR damper. The output of this inverse NN model is the voltage required to produce the desirable control force under the current response condition. This voltage is input to the MR damper which then produces force f acting on the building.

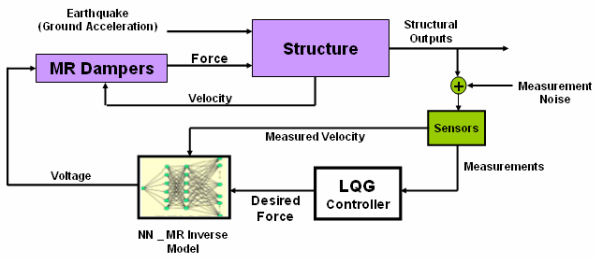

Figure 1: Control Strategy

3.1 MR Model

Adequate modeling of the control devices is essential for the accurate prediction of the behavior of the controlled system. The simple mechanical model shown in Figure 2 was developed and shown to accurately predict the behavior of MR damper over a wide range of inputs [14,16,17]. This phenomenological model was developed based on a previous model used for an MR damper [18]. The equations governing the force f predicted by this model are as follows:

$$f = c_0 \dot{x} + \alpha z \quad (1)$$

$$\dot{z} = \gamma \left| \dot{x} \right| z \left| z \right|^{n-1} - \beta \dot{x} \left| z \right|^{n} + A \dot{x} \quad (2)$$

where z is the evolutionary variable that accounts for the history dependence of the response. The model parameters depend on the voltage v to the current driver as follows:

$$\alpha = \alpha_a + \alpha_b u; \qquad c_0 = c x_{0a} + c_{0b} u \quad (3a, b)$$

where u is given as the output of the first-order filter

$$\dot{u} = -\eta(u - v) \quad (4)$$

Eq. (4) is used to model the dynamics involved in reaching rheological equilibrium and in driving the

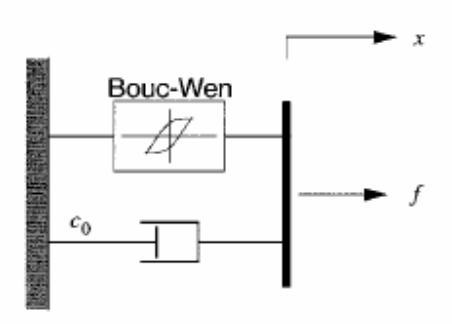

Figure 2: Mechanical model of MR damper

electromagnet in the MR damper [14,16,17]. This MR damper model is used herein to model the behavior of the MR damper.

The parameters of the MR damper were selected so that the device has a capacity of 1,000 kN, as follows: α_a = 1.0872e5 N/cm, α_b = 4.9616e5 N/(cm V), c_{0a} =4.40 N s/cm, c_{0b} =44.0. N s/(cm V), n=1, A=1.2, γ =3 cm^{-1}, β =3 cm^{-1}, and γ =50 s^{-1}.

3.2 Neural network Inverse dynamics of MR damper (NIMR)

The MR damper model discussed earlier in this paper estimates damper forces based on the inputs of the reactive velocity and the issued voltage as described by Equations (1)–(4). The damper velocity is the same as the velocity of the floor the damper is connected to. Thus, the voltage signal is the only parameter that can be modified to control the damper force to produce the required control force. The control algorithm, LQG, estimates the required optimal control force but the MR damper force is controlled by voltage. In such case, it is essential to develop an inverse dynamic model that predicts the corresponding control voltage to be sent to the damper so that an appropriate damper force can be generated. Unfortunately, due to the inherent nonlinear nature of the MR damper, a model like that for its inverse dynamics is difficult to obtain mathematically. Because of this reason, a feed-forward back-propagation neural network is constructed to copy the inverse dynamics of the MR damper (Figure 3) . This model is denoted as NIMR. This neural network model is trained using input-output data generated analytically using the

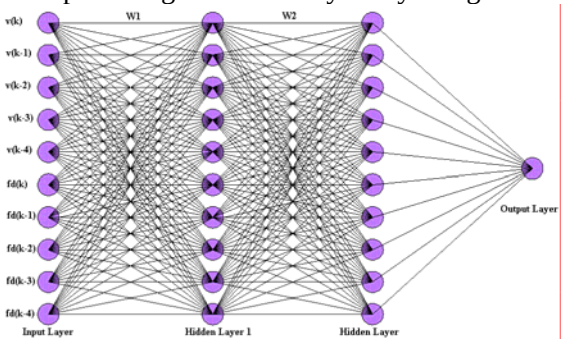

Figure 3: NN of inverse dynamics of MR damper (NIMR)

simulated MR model based on Equations (1)–(4). This NIMR calculates the voltage signal based on the current and few previous histories of measured velocity and desirable control force. Then the voltage signals are sent to the MR damper so that it can generate the desirable optimal control forces. Training the NIMR requires the compilation of input-output data. To completely identify the underlying MR system model, the data must contain information about the entire operating range of the system. Here, in this study, the velocity and voltage are generated randomly using band limited white Gaussian noise. The generated forces are results of the MR model described in Equations (1)–(4). The sampling rate of the training data was 200 Hz for 30 s period, which resulted in 6000 patterns for training, testing and validation , Figure 4. Next step is to select the

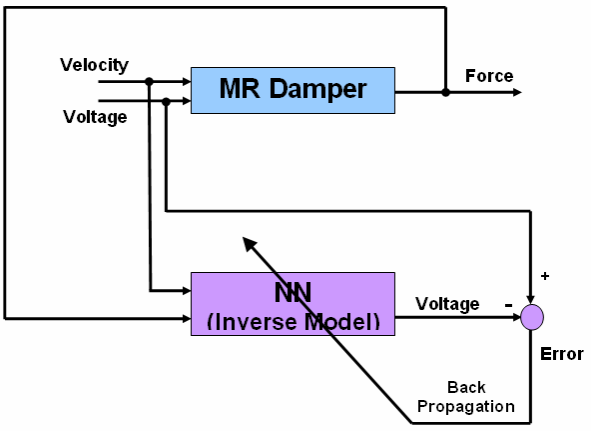

Figure 4: Training of NIMR

network architecture.

To do so it is required to determine the numbers of inputs, outputs, hidden layers, and nodes in the hidden layers, and is usually done by trial and error. The most suitable input data for our case was found to be the current and the four previous histories for the velocity and the force. Also two hidden layers, each layer with ten nodes, were adopted as one of the best suitable topologies for the NIMR as can be seen in Fig. 3. The log-sigmoid (ranging from 0 to 1) activation function is used for the hidden layers and the linear function for the output layer which represents the voltage. 3000 patterns of the provided data was choosen for training which required 1000 training epochs to achieve a mean-square-error (MSE) of 1e−03.

The training is carried out upon the generated data using the Levenberg–Marquardt algorithm [19], which is encoded in Neural Networks Toolbox in MATLAB [20] under 'trainlm' routine. Finally, testing and validation of the trained network is investigated using few sets of new data for a 30 s period. Fig. 5 shows the training testing and validation velocity, forces and voltage records used in constructing the NIMR model. Additionally, Fig. 5 compares the forces computed by MR damper model, based on the generated random voltage, to the forces computed by MR damper model based on the predicted voltages by NIMR. Moreover, the predicted voltage record from the NIMR is compared to the randomly generated targets and presented in Figure 5. It is clear that in general, the predicted voltages are reasonably close to the target voltages. The near perfect match in the training region indicates that the NIMR model is well trained. Henceforth, the NIMR model will be used to compute the required voltage for a specific force and velocity. This will alleviate problems resulting when using control algorithm that computes only the optimal control forces.

3.3 Control Performance

The performance of the NIMR neural network is checked according to comparison of the force generated by MR damper to the ideal force estimated by LQG controller. Figure 6 shows the force generated by the MR damper at first floor of the building for Elcentro earthquake commanded by NIMR as compared to ideal force estimated by LQG controller. It can be seen that the damper forces follow the target optimal control force quite closely.

The performance of the controller is also investigated based on the evaluation criteria specified ($J1$– $J17$) for the 3-story nonlinear benchmark buildings [15]. These criteria which are

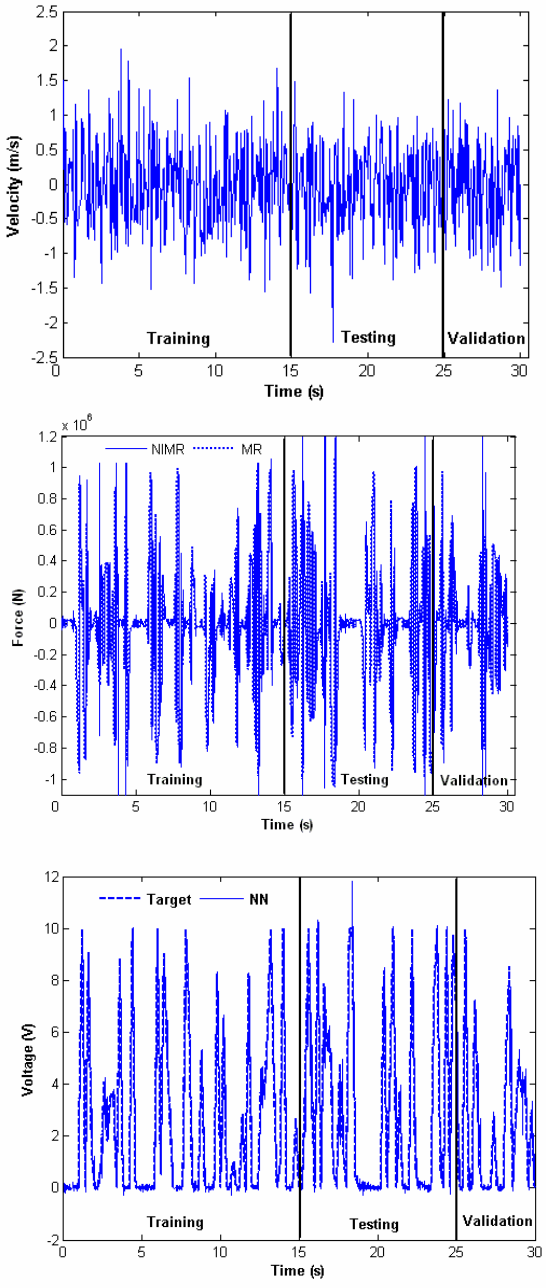

Figure 5: Training ,testing and validation data

briefly presented in table 1, are calculated as a ratio of the controlled and the uncontrolled responses in most cases. Ten earthquake records are used in the simulation, using the original four earthquake records with different intensities. These records are the El Centro and Hachniohe earthquake records with 0.5, 1.0, and 1.5 intensity, and Northridge and Kobe earthquake records with 0.5 and 1.0 intensity.. to make a comparison, an active control system and semi-active clipped-optimal control (COC) system [4], are also designed. Table 2 presents the evaluation criteria as the ratio of the controlled response to the uncontrolled response for each earthquake record individually for active, COC and the proposed control algorithms. Figure 7 also shows the relative performance of the three algorithms for criteria J1, J2 and J3.The results show that NIMR controller performs better than CQC and active control to reduce the peak drift ratio ($J1$) for eight of the earthquake records. For the peak level acceleration ($J2$), the NIMR controller has been able to perform better or equal to CQC for seven of the ten earthquake records., The peak base shear force criterion ($J3$) for NIMR is smaller than CQC for seven of the earthquake records and smaller than active for five of them. In terms of norm drift ratio ($J4$), the performance of NIMR is better for seven earthquake records and for two of them the response is equal or worse. The NIMR is more effective in reduction of norm level acceleration ($J5$) and the norm base shear force ($J6$) for eight of earthquake records. In terms of building damage criteria ($J7$– $J10$), the NIMR controller has the ability to reduce the ductility ratio ($J7$) more for

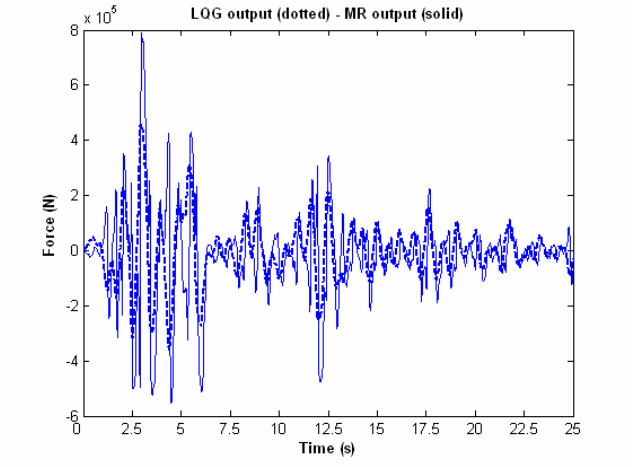

Figure 6: comparison of the force generated by MR damper to the ideal force (LQG)

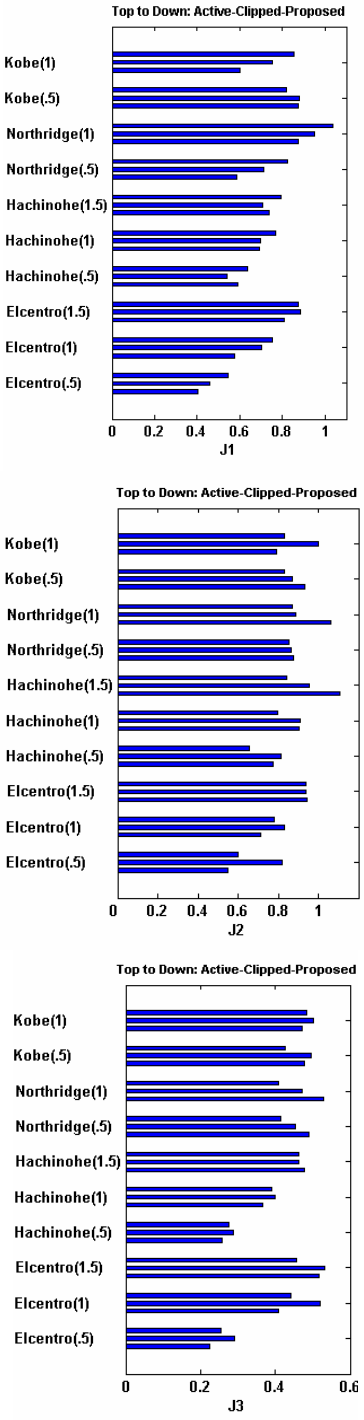

Figure 7: Comparison of performance criteria J1-J3 of NIMR to active and COC method

Table 1: Performance criteria for seismically excited nonlinear building

Interstory Drift Ratio $J_1 = \max_{\text{El Centro, Hachinohe, Northridge, Kobe}} \left\{ \frac{\max_{t,i} \frac{\lvert d_i(t) \rvert}{h_i}}{\delta^{\max}} \right\}$	**Level Acceleration** $J_2 = \max_{\text{El Centro, Hachinohe, Northridge, Kobe}} \left\{ \frac{\max_{t,i} \lvert \ddot{x}_{ai}(t) \rvert}{\ddot{x}_a^{\max}} \right\}$	**Base Shear** $J_3 = \max_{\text{El Centro, Hachinohe, Northridge, Kobe}} \left\{ \frac{\max_{t} \lvert \sum_i m_i \ddot{x}_{ai}(t) \rvert}{F_b^{\max}} \right\}$
Normed Interstory Drift Ratio $J_4 = \max_{\text{El Centro, Hachinohe, Northridge, Kobe}} \left\{ \frac{\max_{i} \frac{\lVert d_i(t) \rVert}{h_i}}{\lVert \delta^{\max} \rVert} \right\}$	**Normed Level Acceleration** $J_5 = \max_{\text{El Centro, Hachinohe, Northridge, Kobe}} \left\{ \frac{\max_{i} \lVert \ddot{x}_{ai}(t) \rVert}{\lVert \ddot{x}_a^{\max} \rVert} \right\}$	**Normed Base Shear** $J_6 = \max_{\text{El Centro, Hachinohe, Northridge, Kobe}} \left\{ \frac{\lVert \sum_i m_i \ddot{x}_{ai}(t) \rVert}{\lVert F_b^{\max} \rVert} \right\}$
Ductility $J_7 = \max_{\text{El Centro, Hachinohe, Northridge, Kobe}} \left\{ \frac{\max_{t,j} \frac{\lvert \phi_j(t) \rvert}{\phi_{yj}}}{\phi^{\max}} \right\}$	**Dissipated Energy** $J_8 = \max_{\text{El Centro, Hachinohe, Northridge, Kobe}} \left\{ \frac{\max_{t,j} \int dE_j}{F_{yj} \cdot \phi_{yj}} \right\}$	**Plastic Connections** $J_9 = \max_{\text{El Centro, Hachinohe, Northridge, Kobe}} \left\{ \frac{N_d^C}{N_d} \right\}$
Normed Ductility $J_{10} = \max_{\text{El Centro, Hachinohe, Northridge, Kobe}} \left\{ \frac{\max_{j} \frac{\lVert \phi_j(t) \rVert}{\phi_{yj}}}{\lVert \phi^{\max} \rVert} \right\}$	**Control Force** $J_{11} = \max_{\text{El Centro, Hachinohe, Northridge, Kobe}} \left\{ \frac{\max_{t,j} \lvert f_j(t) \rvert}{W} \right\}$	**Control Device Stroke** $J_{12} = \max_{\text{El Centro, Hachinohe, Northridge, Kobe}} \left\{ \frac{\max_{t,i} \lvert y_i^a(t) \rvert}{x^{\max}} \right\}$
Control Power $J_{13} = \max_{\text{El Centro, Hachinohe, Northridge, Kobe}} \left\{ \frac{\max_{t} \left[\sum_i \mathcal{P}_i(t) \right]}{\dot{x}^{\max} W} \right\}$	**Normed Control Power** $J_{14} = \max_{\text{El Centro, Hachinohe, Northridge, Kobe}} \left\{ \frac{\sum_i \frac{1}{t_f} \int_0^{t_f} \mathcal{P}_i(t)}{\dot{x}^{\max} W} \right\}$	**Control Devices** J_{15} = Number of control devices **Sensors** J_{16} = Number of required sensors **Computational Resources** $J_{17} = \dim(\mathbf{x}_k^c)$

eight of the earthquake records. For the dissipated energy ($J8$), and the plastic connection ratio ($J9$) NIMR is more effective for all cases except for one (Kobe 1). For the norm ductility ratio ($J10$), the performance is similar to the ductility ratio. In terms of control devices and control requirement criteria, the performance of the NIMR controller appears to be reasonable.

4 Conclusion

In this study, neural networks are used to model the inverse dynamics of MR damper. The inputs to the NN models are a few time steps of structural velocities and damper forces. The output is the command voltage to the MR damper. These NN models estimate the voltage that is required to produce a target control force calculated from some optimal control algorithms. The main objective of this development is to explore whether the semi-active MR damper can be used to produce optimal control forces.

A 3-story nonlinear benchmark building has been used for study. The results illustrate that it is possible to incorporate the NN models into the control strategy and hence operate the damper in an active mode. In general, the forces generated by the MR damper can follow those calculated from the optimal control algorithms. The performance of the controller has been checked based on the evaluation criteria specified ($J1$– $J17$) for the benchmark building. The results show that the NIMR controller in most cases perform better than CQC and active controller.

Table 2: Performance criteria for active, clipped optimal control(CQC) and NIMR algorithms

		Elcentro 0.5	Elcentro 1	Elcentro 1.5	Hachino 0.5	Hachino 1	Hachino 1.5	Nortdrige . 5	Nortdrige 1	Kobe 0.5	Kobe 1
J1	NIMR	0.40553	0.57479	0.80675	0.59193	0.68943	0.73614	0.58348	0.87394	0.87558	0.60275
	COC	0.45736	0.70362	0.88271	0.54134	0.6969	0.70556	0.7138	0.94951	0.88084	0.75219
	ACTIVE	0.54424	0.75285	0.87259	0.6365	0.7676	0.79386	0.82554	1.0353	0.81943	0.85444
J2	NIMR	0.54759	0.7122	0.94337	0.77719	0.90286	1.1082	0.87511	1.0601	0.93323	0.7911
	COC	0.82026	0.82887	0.93809	0.81202	0.90876	0.95677	0.86246	0.88956	0.87056	1.0016
	ACTIVE	0.59765	0.78135	0.93931	0.65844	0.79755	0.8442	0.85077	0.86931	0.82948	0.83332
J3	NIMR	0.22588	0.40835	0.51832	0.25902	0.36656	0.47714	0.48877	0.52848	0.4791	0.47237
	COC	0.2914	0.52142	0.53091	0.2868	0.39837	0.46139	0.45505	0.47133	0.49679	0.50292
	ACTIVE	0.25331	0.44034	0.45696	0.2765	0.38941	0.46256	0.41536	0.40973	0.42569	0.48287
J4	NIMR	0.65207	0.65486	0.65419	0.45959	0.44222	0.73624	0.1734	0.66228	1.5245	1.0497
	COC	0.65597	0.77567	0.69309	0.35236	0.47129	0.95616	0.70967	1.1988	1.1487	1.5761
	ACTIVE	0.79921	0.85123	0.70811	0.58972	0.65482	1.1991	1.0876	1.2366	0.82856	1.2015
J5	NIMR	0.75359	0.83806	0.88108	0.52317	0.54288	0.62637	0.82816	0.90583	0.74291	0.87799
	COC	0.78085	0.94497	0.93176	0.57	0.56511	0.70436	0.861	0.88682	0.79421	0.91513
	ACTIVE	0.7639	0.93121	0.92534	0.56115	0.68506	0.81406	0.87825	0.91388	0.82083	0.92598
J6	NIMR	0.36682	0.41342	0.43452	0.26724	0.27845	0.32312	0.46945	0.48184	0.36809	0.45932
	COC	0.37679	0.46562	0.45621	0.22983	0.28911	0.36129	0.48128	0.47431	0.39601	0.46842
	ACTIVE	0.37041	0.45527	0.44624	0.2786	0.34098	0.40652	0.47643	0.4683	0.39017	0.45502
J7	NIMR	0.37786	0.47835	0.70369	0.53109	0.50499	0.64341	0.38215	0.75047	0.90107	0.72183
	COC	0.42239	0.62548	0.76103	0.4947	0.5224	0.72603	0.66578	0.84398	0.8728	0.83382
	ACTIVE	0.51178	0.68052	0.79809	0.59302	0.58167	0.76975	0.80358	0.89743	0.80839	0.85556
J8	NIMR	1.50E-08	3.01E-10	0.17243	0	1.86E-11	0.018669	0.10496	0.63037	0.34414	0.87795
	COC	9.16E-06	0.02394	0.35026	0	6.54E-07	0.054856	0.5641	0.74859	0.53341	0.90693
	ACTIVE	3.37E-05	0.1362	0.39675	0	0.000230	0.049153	0.91967	0.93195	0.48192	0.77793
J9	NIMR	0	0	1	0	0	0.83333	0.25	0.84848	0.91667	0.875
	COC	0	0.36364	1	0	0	0.91667	0.58333	0.84848	0.91667	0.9375
	ACTIVE	0	0.54545	1	0	0.090909	0.91667	1	0.93939	0.91667	0.875
J 10	NIMR	0.44032	0.28809	0.38866	0.32493	0.2667	0.55459	0.078523	0.57843	1.2321	0.80763
	COC	0.43696	0.36044	0.43023	0.25171	0.28596	0.83656	0.57177	1.0125	1.0132	1.3432
	ACTIVE	0.54222	0.43081	0.5387	0.42046	0.39788	0.85147	0.83826	1.0246	0.71108	0.86511
J 11	NIMR	0.019819	0.033001	0.035661	0.018251	0.027726	0.033545	0.03572	0.036279	0.035383	0.036187
	COC	0.020579	0.029049	0.033333	0.018398	0.02796	0.032568	0.034488	0.035894	0.029902	0.035369
	ACTIVE	0.011308	0.022655	0.026862	0.0093158	0.019031	0.02547	0.028587	0.034567	0.025089	0.029868
J 12	NIMR	1.0933	1.6098	2.2671	1.243	1.8995	2.1983	2.1345	2.4451	2.2143	2.3436
	COC	1.34	1.8301	2.267	1.6703	1.5617	1.7076	2.0771	2.1993	1.6315	2.0523
	ACTIVE	0.21643	0.29754	0.34443	0.24427	0.30079	0.34751	0.36128	0.38213	0.33538	0.40294
J 13	NIMR	0.3707	0.87578	0.9207	0.40785	0.67359	0.974	0.86818	0.85595	0.77949	0.64927
	COC	1.2417	1.4262	1.2981	1.383	1.4329	1.7577	1.533	1.1599	1.2495	0.89283
	ACTIVE	0.010545	0.033184	0.033727	0.0088538	0.02167	0.034063	0.042317	0.051224	0.03942	0.042638
J 14	NIMR	0.0095514	0.031347	0.048565	0.013386	0.032363	0.064078	0.018005	0.031561	0.013155	0.019664
	COC	0.036857	0.059435	0.063976	0.054362	0.063053	0.093657	0.029852	0.03903	0.020539	0.023319
	ACTIVE	0.0003363	0.0010777	0.001554	0.0004745	0.001138	0.0023126	0.0005768	0.0011768	0.0004883	0.0008078

References

[1] Casciati, F., Magonette, G., and Marazzi, F., *Technology of semi-active devices and application in vibration mitigation.* John-Wiley, 2006.

[2] Sack, R. L., Kuo, C. C., Wu, H. C., Liu, L., and Patten, W. N.. ‘‘Seismic motion control via semi-active hydraulic actuators.’’ *Proc., U.S. 5th Nat. Conf. on Earthquake Engrg.*, Vol. 2, Oakland, Calif., PP. 311–320, 1994.

[3] Sack, R. L., and Patten, W. ‘‘Semi-active hydraulic structural control.’’ *Proc., Int. Workshop on Struct. Control*, Los Angeles, PP. 417–431, 1994.

[4] Dyke, S. J., Spencer, B. F., Jr., Sain, M. K., and Carlson, J. D., ‘‘Seismic response reduction using magnetorheological dampers.’’ *Proc., IFAC World Congr.*, PP. 145–150, 1996c.

[5] Dyke, S. J., Spencer, B. F., Jr., Sain, M. K., and Carlson, J. D., ‘‘Modeling and control of magnetorheological dampers for seismic response reduction.’’ *Smart Mat. and Struct.*, Vol. 5, PP. 565–575, 1996d.

[6] Yoshida1, O. Dyke, S., "Seismic Control of a Nonlinear Benchmark Building Using Smart Dampers", *Journal of Engineering Mechanics (ASCE*). Vol. 130, No.4, PP. 386–392, 2004.

[7] Lee H. J., Yang Y. G., Jung H. J.,Spencer B. F., and Lee I. W., “Semi-active neurocontrol of a base-isolated benchmark structure”, *Struct. Control Health Monit,* Vol. 13, PP. 682–692, 2006.

[8] Bani-Hani K. A., and Mashal A. Sheban M. A.,
“Semi-active neuro-control for base-isolation system using magnetorheological (MR) dampers”, *Earthquake Engng Struct. Dyn*. Vol. 35, PP. 1119–1144, 2006.

[9] Jung H. J., Lee H. J., Yoon W. H., Oh J. W. and Lee I. W., “Semiactive Neurocontrol for Seismic Response Reduction Using Smart Damping Strategy”, *Journal of Computing in Civil Engineering*, Vol. 18, No. 3, PP. 277-280, 2004.

[10] Choi K-M, Cho S-W, Jung H-J, Lee I-W, “Semi-active fuzzy control for seismic response reduction using magnetorheological dampers” , *Earthquake Engng Struct. Dyn*. Vol. 33, PP. 723–736, 2004.

[11] Bhardwaj M. K., and Datta T. K., “Semiactive Fuzzy Control of the Seismic Response of Building Frames”*Journal of Structural Engineering*, Vol. 132, No. 5, PP. 791-799, 2006.

[12] Kim H-S., and Roschke P. N., “GA-fuzzy control of smart base isolated benchmark building using supervisory control technique”, *Advances in Engineering Software* Vol. 38, PP. 453–465, 2007.

[13] Chang C-C, Zhou L. “Neural network emulation of inverse dynamics for a magnetorheological damper.”, *Journal of Structural Engineering* , Vol. 128, No. 2, PP. 231–239, 2002.

[14] Dyke, S. J., Yi, F., and Carlson, J. D. (1999). “Application of magnetorheological dampers to seismically excited structures.”, *Proc., Int. Modal Anal. Conf.*, Bethel, Conn, 1999..

[15] Ohtori, Y., Christenson, R. E., Spencer, B. F., Jr., and Dyke, S. J., “Benchmark control problems for seismically excited nonlinear buildings.” *J. Eng. Mech.,* Vol. 130, No. 4, PP. 366–387, 2004..

[16] Yi, F., Dyke, S. J., Caicedo, J. M., and Carlson, J. D., “Seismic response control using smart dampers.” *Proc., 1999 Am. Control Conf.*, Washington, D.C., PP. 1022–1026, 1999.

[17] Yi, F., Dyke, S. J., Frech, S., and Carlson, J. D., “Investigation of magnetorheological dampers for earthquake hazard mitigation.” *Proc., 2nd World Conf. on Struct. Control*, West Sussex, U.K., PP. 349–358, 1998.

[18] Spencer, B. F., Jr., Dyke, S. J., Sain, M. K., and Carlson, J. D., “Phenomenological model of magnetorheological damper.” *J. Engrg. Mech.*, ASCE, Vol. 123, No. 3, PP. 230–238, 1997.

[19] Hertz J, Krogh A, Palmer RG. “*Introduction to the Theory of Neural Computation*”, Addison-Wesley Publishing Company: Boston, MA, 1993.

[20] The Math Works Inc. *MATLAB 7.0*, Natick, MA, 2006.